Editor's Choice: Separations: Materials, Devices and Processes

# Mixed-Cation LiCa-LSX Zeolite with Minimum Lithium for Air Separation

**Franklin E. Epiepang and Ralph T. Yang**
Dept. of Chemical Engineering, University of Michigan, Ann Arbor, MI 48109

**Xiong Yang**
Dept. of Chemical Engineering, University of Michigan, Ann Arbor, MI 48109

School of Energy and Environmental Engineering, University of Science and Technology Beijing, Beijing 100083 China

**Jianbo Li**
Luoyang Jianlong Micro-Nano New Materials Co., Ltd., Yangshi City, Henan Province 471900, China

**Yingshu Liu**
School of Energy and Environmental Engineering, University of Science and Technology Beijing, Beijing 100083 China

*DOI 10.1002/aic.16032*
*Published online December 1, 2017 in Wiley Online Library (wileyonlinelibrary.com)*

*The aim of this work was to reduce/minimize Li in Li-LSX by replacing the 70% $Li^+$ cations in Li-LSX that are bonded to the interior or inaccessible sites which are not used for adsorption. Thus, mixed-cation LiCa-LSX containing minimum lithium were prepared by exchanging small fractions of $Li^+$ into Ca-LSX, followed by dehydration under mild conditions to avoid migration/equilibration of Li cations. Comparisons of adsorption isotherms of $N_2/O_2$ and heats of adsorption for the LiCa-LSX samples with that for pure-cation Li-LSX and Ca-LSX provided strong evidence that significant amounts of these Li cations indeed remained on the exposed sites (SIII). The mixed-cation LiCa-LSX samples were compared against the pure-cation Ca-LSX and Li-LSX based on their performance for oxygen production by PSA, via model simulation. The results showed that the mixed-cation LiCa-LSX samples yielded significantly higher $O_2$ product productivities at the same product purity and recovery than their pure-cation precursor (Ca-LSX).* © 2017 American Institute of Chemical Engineers *AIChE J*, 64: 406–415, 2018

*Keywords: air separation, mixed-cation exchanged zeolite, LiCa-LSX for air separation, Li-LSX*

## Introduction

The demand for oxygen and nitrogen spans over a wide range of industries including oil refining, medical, metal production, food processing, and chemicals to name a few. Cryogenic distillation of liquefied air and pressure swing adsorption (PSA) are the two major technologies for high and low-to-medium volume productions, respectively.[1]

Air separation by adsorption is based on the unique adsorption property of zeolites which have high $N_2/O_2$ selectivities due to the interactions between the electric field gradient of the zeolitic cation and the quadrupole moment of $N_2$.[2] Commercial PSA oxygen production began in 1972. A major breakthrough occurred in 1989 with the invention of Li-LSX (i.e., low silica type-X, Si/Al = 1) zeolite by Chao.[3] In the preparation of Li-LSX, the as-synthesized Na-LSX is ion-exchanged by Li cations via conventional means. It was found that below approximately 70% Li exchange, the $N_2$ capacity was unchanged, while it increased nearly linearly upon further increase in Li exchange from 70 to 100%. This phenomenon has been explained by the occupancy of different cation sites; the $N_2$ (and $O_2$) molecules can interact only with cations occupying the exposed sites. The cation sites for faujasite are shown in Figure 1. For Li-X, only sites III (SIII) are accessible to $N_2$ (and $O_2$); $Li^+$ on SII is not "accessible" due to electron shielding effects by the surrounding framework oxygen and the small size of the Li ion.

The site occupancies have been characterized[4–6] and are shown in Table 1. It is noted that, after ion exchange, zeolites need to be thermally dehydrated prior to isotherm measurements (and during manufacturing), typically at above 673 K for four or more hours. Under such treatment, cations migrate or diffuse to their equilibrium positions or sites. For zeolites containing mixed cations, it has long been observed that the lighter cations tend to migrate to the lower numbered sites (SI, SI′, SII″, SII). For example, in mixed CeNaCa-X zeolite, Na

Additional Supporting Information may be found in the online version of this article.

Correspondence concerning this article should be addressed to R. T. Yang at yang@umich.edu.

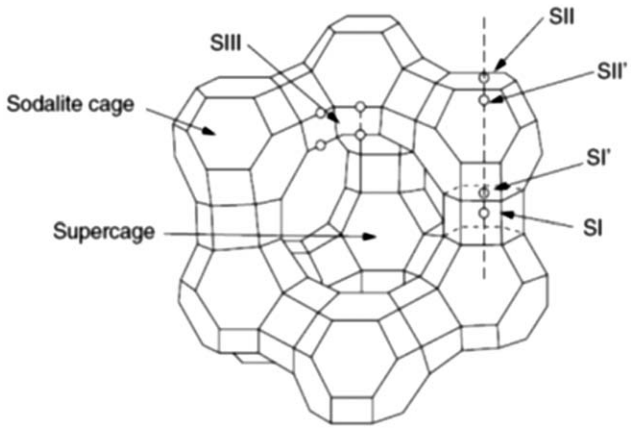


**Figure 1. Unit cell of faujasite-type (X and Y) zeolites, including cation sites.[2]**

and Ca are at lower-numbered sites while Ce(III) cations are located at outer sites, and in mixed NaSr-X zeolite, $Na^+$ is at SI while $Sr^{2+}$ is at SII.[7] This ordering is also seen in the mixed LiNa-LSX system discussed above.

As mentioned, since its invention Li-LSX has been the sorbent of choice for air separation by PSA or vacuum swing adsorption (VSA). A wide variety of other zeolites have also been considered, particularly the LSX zeolites containing alkali-earth metal cations. These cations are divalent and hence they form strong electrostatic interactions with $N_2$ molecules (as well as $O_2$). Thus, intense interests were attracted to the mixed-cation LSX zeolites containing Li and an alkali-earth metal.[8–13] Coe et al.[8–11] studied various binary exchanged X-zeolites containing varying lithium-calcium and lithium-strontium mixtures all of which provided enhanced nitrogen sorption capacities over those of the pure samples. Sircar et al.,[12] also showed a binary ion-exchanged Type-X zeolite of calcium and strontium. Their invention was especially useful in the adsorption of $N_2$ from an air stream at superambient pressure to produce an $O_2$-rich product stream. Furthermore, Chao et al.,[13] presented mixed ion-exchanged zeolites of type-A and type-X with lithium (30–90%) and alkaline earth metals (10–70%) such as $Ca^{2+}$ and $Sr^{2+}$, with high $N_2$ adsorption capacity. It is important to note that these mixed-cation zeolites required over 70 mol% $Li^+$ (and <30 mol% alkali-earth cation). Typically, 90% $Li^+$ was required. Moreover, it was necessary to ion exchange $Li^+$ first, followed by exchange for the alkali earth cations. Of particular interest was the Ca-LSX zeolite[14] due to its high $N_2$ capacities over that of Li-LSX. Thus, for mixed-cation LiCa-LSX, it was specifically stated that fully exchanged Li-LSX was prepared first, followed by $Ca^{2+}$ exchange.[8,10,13] In all cases, well over 70% $Li^+$ was needed to see the effect of $Li^+$.

**Table 1. Cation Site Occupancies in Dehydrated X Zeolites (Maximum = 96 Monovalent Cations per Unit Cell for Si/Al = 1)**

| Zeolite | Al/unit cell | Sites | | | | |
|---|---|---|---|---|---|---|
| | | I | I′ | II | II′ | III |
| **Li-LSX[24]** | 95.8 | | 27.2 | 33.9 | | 32.4 |
| **Li-LSX[25]** | 96 | | 33 | 34 | | 29 |
| **Na-X (13X)[26]** | 81 | 3.8 | 32.3 | 30.8 | | 7.9 |
| **K-X[27]** | 87 | 9 | 13 | 26 | | 38 |
| **Ca-X[28]** | 86 | 7.5 | 17.3 | 17.3 | 9.0 | |

The demand for lithium has been rising steeply due to the application of lithium ion batteries for energy storage and due to its limited reserves worldwide. As a result, the price of lithium has been surging since 2016 while the reserve is dwindling. Therefore, the motivation for this work is to develop zeolites for air separation in which lithium is substantially reduced or replaced by a low-cost and abundant alkali-earth metal cation, such as $Ca^{2+}$. Using LiCa-LSX as an example, our strategy is to first exchange as-synthesized Na-LSX to fully-exchanged Ca-LSX, followed by exchange of a small fraction of $Ca^{2+}$ by $Li^+$. During the ion exchange process (in an aqueous solution such as $LiCl_2$) and prior to any heat treatment, it is reasonable to assume that these $Li^+$ cations are located on SIII because they are the most accessible ion exchange sites and are hence exchanged first. Equally important, in this work the dehydration step is performed at the lowest possible temperature in a relatively short time to avoid diffusion and equilibration of Li ions to lower-number or interior sites.

In this work, we focused on four synthetic zeolites: two pure-cation zeolites (Ca-LSX and Li-LSX) and two mixed-cation zeolites (2.5% LiCa- and 4.2% LiCa-LSX, both in mol%) for the PSA/VSA system. The mixed-cation samples will be represented as follows henceforth: 2.5% LiCa-LSX and 4.2% LiCa-LSX = $Li_{2.5}Ca_{46.75}$-LSX and $Li_{4.2}Ca_{45.9}$-LSX, respectively. These zeolites will be compared for their PSA/VSA separation performance using a proven PSA model.

## Experimental Section

### *Materials*

The analysis gases obtained from Cryogenic Gases included: helium (99.995%, prepurified), nitrogen (99.998%, prepurified), and oxygen (99.6%, extra dry).

Luoyang Jianlong micro-Nano New materials Co., Ltd., China, supplied the Na-LSX zeolite (powder form) with a Na exchange extent of 99.5% (Na/(Na + K) and a Si/Al ratio of 1.005. Calcium dihydrate 99% and lithium chloride 99% were both obtained from Sigma Aldrich.

### *Preparation of Ca-LSX zeolite*

Na-LSX zeolite was used as the starting sorbent for the ion-exchange procedure which could be readily exchanged with most cations. To obtain pure Ca-LSX zeolite, Na-LSX was ion-exchanged with a 1.0 M solution of calcium chloride (with ~3 equivalent excess of $Ca^{2+}$ to $Na^+$) at ambient conditions and stirred for a minimum of 6 h. The solution was decanted and a 3× $CaCl_2$ solution was added, and the ion-exchange procedure was repeated six times. The sample was vacuum filtered after the final ion-exchange, washed with copious amounts of deionized water, and air dried at 298 K for 24 h. One of the main differences between this study and other published literature[8,14] is the fact that here-in, Li ions are introduced into Ca-LSX as opposed to Ca cations being incorporated into Li-LSX zeolite.

### *Preparation of LiCa-LSX*

A pre-determined equivalent amount of $Li^+$ enough to exchange the desired target $Ca^{2+}$ in the Ca-LSX zeolite (assuming hypothetically that all $Li^+$ would undergo exchange) was used to prepare the mixed-cation samples. This

**Table 2. Composition of Various Represented Sorbents**

| | Mole ratio | | | |
|---|---|---|---|---|
| Zeolite | Si/Al | Li/Al | Ca/Al | Na/Al |
| **Na-LSX** | 1.005 | – | – | 0.995 |
| **Ca-LSX** | 1.005 | – | 0.991 | – |
| **$Li_{2.5}Ca_{46.75}$-LSX** | 1.005 | 0.025 | 0.467 | – |
| **$Li_{4.2}Ca_{45.9}$-LSX** | 1.005 | 0.042 | 0.459 | – |

was achieved by using a 0.1 M LiCl solution exchanged with 1.5 g of Ca-LSX with $Li^+$ equivalent = 0.15 and 0.3. The mixture was stirred for 1 h at 298 K followed by vacuum filtration without washing and dried in an oven for 24 h at 298 K. It should be noted that, due to the preference of LSX for $Ca^{2+}$ over $Li^+$, the actual $Li^+$ exchange was substantially less than the amount of $Li^+$ in the liquid phase, as determined by ICP results.

### *Sample pretreatment and isotherm measurements*

All pure gas adsorption equilibrium analysis on the studied pure and mixed ion-exchanged samples were carried out with a Micromeritics ASAP 2020 Sorptometer which uses the volumetric measurement technique. Prior to analysis, all samples were degassed/dehydrated in-situ the Micromeritics to remove all adsorbed moisture and/or adsorbed gasses.

The pretreatment conditions varied per sample and were as follows: 8 h at 648 and 623 K for Li-LSX and Ca-LSX, respectively. 1 h at 623 K for $Li_{2.5}Ca_{46.75}$-LSX and $Li_{4.2}Ca_{45.9}$-LSX while the ramp rate for all dehydration conditions was 283 K/min. The 1 h at 623 K pretreatment condition allows most of the theoretically determined $Li^+$ to remain on site III while not allowing adequate time for all $Li^+$ cations to diffuse to the lower-numbered sites (SI and SII). The temperature of 623 K was determined to be the lowest temperature that was adequate for full dehydration of Li-LSX.[15] In the work of Hutson et al., residual water amounts and $N_2$ isotherms were measured on Li-LSX after dehydration at various temperatures up to 723 K, and full dehydration was seen after dehydration at 623 K.[15] All studied samples were pretreated under vacuum: 30 $\mu$mHg for the pure samples and 60 $\mu$mHg (due to the short pretreatment time) for the mixed samples.

### *Sample characterization*

The samples were compositionally characterized using an ICP-OES (inductively coupled plasma—optical emission spectrometer) system at Galbraith Laboratories Inc. in Knoxville, Tennessee. ICP is an analytical technique that quantifies the elemental composition of samples in various states (e.g., powders, liquids, suspensions, etc.). Powders are usually digested by an acid (highly concentrated $HNO_3$, HCl, or $H_2SO_4$) or a combination of acids with the resulting solution then nebulized into the core of the instrument's inductively coupled argon plasma at elevated temperatures. The high temperature vaporizes, ionizes and thermally excites the analyte species in the solution which are then detected and quantified by the OES by measuring (in % or ppm concentration) the element's characteristic wavelength from the intensity of the emitted radiation.

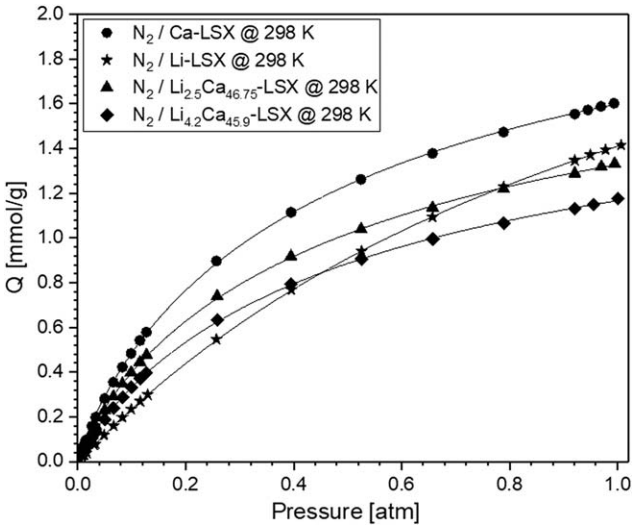


**Figure 2. Experimental adsorption isotherms of $N_2$ at 298 K and 101 kPa on representative sorbents.**

## Results and Discussion

### *Analytical sample characterization*

As mentioned above, the mixed ion-exchanged samples were compositionally analyzed and quantified for Li and Ca content using an inductively coupled plasma—optical emission spectroscopy (ICP-OES) system. The extent of the $Li^+$ exchange obtained from the mixed ion-exchanged samples by ICP were 2.5% Li and 4.2% Li (mole percent and on a dry basis) represented as $Li_{2.5}Ca_{46.75}$-LSX and $Li_{4.2}Ca_{45.9}$-LSX, respectively. The results of the analyzed LSX sample are presented in Table 2.

### *Nitrogen adsorption isotherms*

As stated earlier, the volumetric technique was used to measure the equilibrium $N_2$ adsorbed amounts to pressures of 1 atm. $N_2$ experimental adsorption isotherms on the studied sorbents at temperatures 298, 323, and 343 K after in vacuo dehydration are shown in Figures 2–4, respectively. Upon

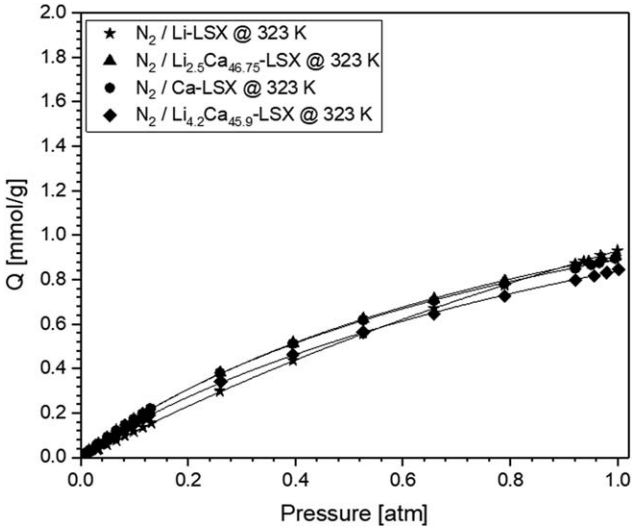


**Figure 3. Experimental adsorption isotherms of $N_2$ at 323 K and 101 kPa on representative sorbents.**

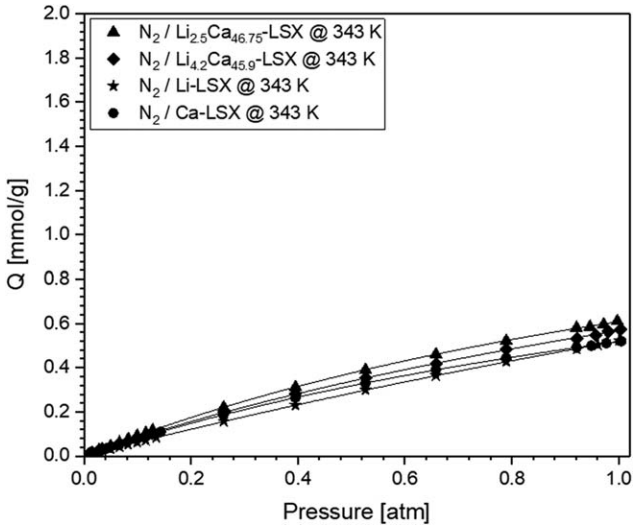


**Figure 4. Experimental adsorption isotherms of $N_2$ at 343 K and 101 kPa on representative sorbents.**

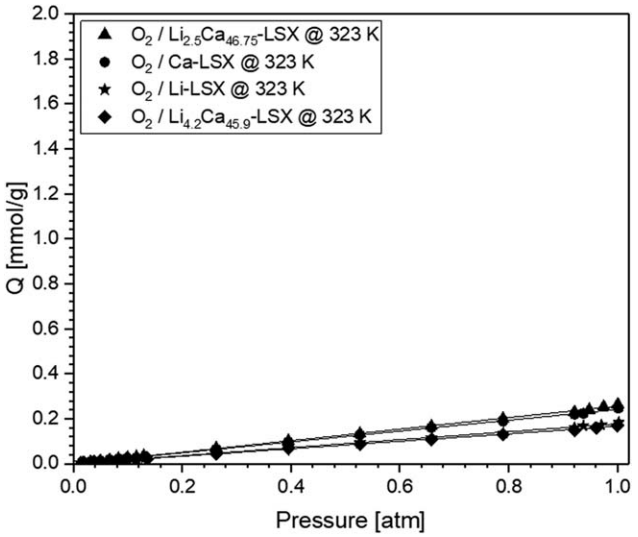


**Figure 6. Experimental adsorption isotherms of $O_2$ at 323 K and 101 kPa on representative sorbents.**

inspection, Ca-LSX shows the highest $N_2$ adsorption capacity followed by $Li_{2.5}Ca_{46.75}$-LSX and $Li_{4.2}Ca_{45.9}$-LSX at ambient conditions, respectively. The pure Ca-LSX sample shows a high capacity for $N_2$ at 298 K in comparison with other published data.[2,8] Figure 2 ($N_2$ isotherms at 298 K and 101 kPa) also reveals that the introduction of such low Li amounts changes the adsorptive properties (low pressure knee of the pure zeolite) of the mixed-cation zeolite. The sorbents' high $N_2$ capacities are attractive properties for air separation by PSA.

### *Oxygen adsorption isotherms*

Figures 5–7 show $O_2$ experimental adsorption isotherms on the studied sorbents at 298, 323, and 343 K, respectively. A comparison of the different sorbents shows that Ca-LSX adsorbed significantly more oxygen than Li-LSX (slightly above 60%), and the mixed-cation LSX fell in between. This result is expected because $Ca^{2+}$ has higher polarizability than $Li^+$ and the van der Waals interactions were the main interactions for adsorption of $O_2$ which has a very low quadrupole moment. The lower $O_2$ capacities for the mixed-cation LSX are favorable for PSA separation. This result also indicates the presence of some $Li^+$ cations on SIII in the mixed-cation samples.

It should be noted that the differences in adsorption capacities of both gases on the studied sorbents are due to the magnitude of interactions between the $Ca^{2+}$, $Li^+$ and the sorbates which in turn are due to the location of the cations within the zeolite's framework. Figure 1 shows the five different cation sites in the faujasite-type (X and Y) zeolites. It should be noted that only sites II and III (SII and SIII) are accessible to the sorbate while SI (inside the double ring) and SII' (within the beta cage) are inaccessible to the sorbate molecule. As mentioned, the electric field around the cations in the exposed sites are however, partially shielded (cation size dependent) by the surrounding oxygen atoms thereby significantly lowering

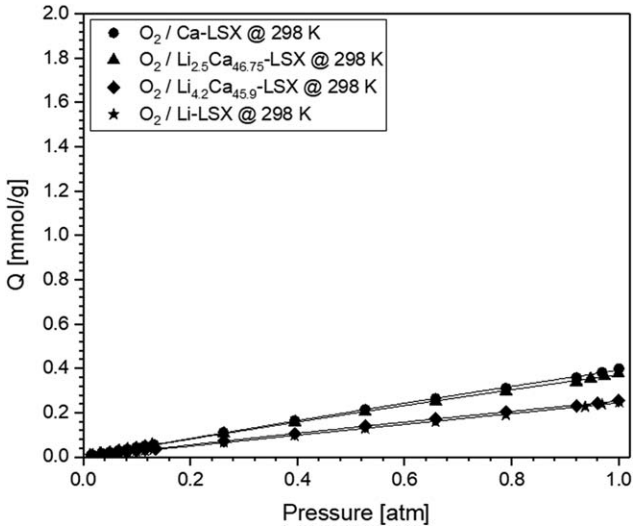


**Figure 5. Experimental adsorption isotherms of $O_2$ at 298 K and 101 kPa on representative sorbents.**

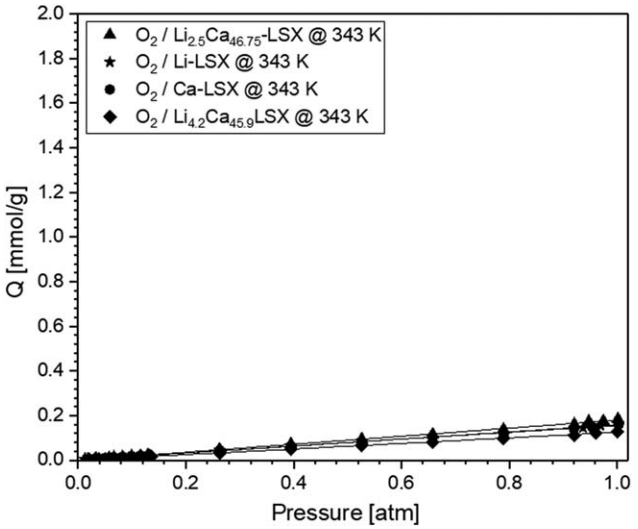


**Figure 7. Experimental adsorption isotherms of $O_2$ at 343 K and 101 kPa on representative sorbents.**

the interactions between the sorbate molecule and the SII cations. For example, the small Li cation can sit crystallographically very low within the face of the single six-ring (SII), allowing the electric field to be nearly completely shielded by the six surrounding framework oxygen atoms thereby allowing the sorbate–sorbent energy to be entirely contributed by the Li cation sitting on SIII.[2] For a larger cation like Ca, its shielding can be substantially weaker due to its size.

### *Pure component isotherms*

The equilibrium adsorption isotherms of $N_2$ and $O_2$ on the various sorbents in this study were fitted with the Langmuir-Freundlich (L-F) isotherm model. Figures 2–7 show just a few of the experimentally obtained isotherms. All others could be found in the Supporting Information. The temperature dependence of the isotherms allowed calculation for the isosteric heats of adsorption, as to be discussed further below.

$$Q = \frac{Q^*_{sat} K C^n}{1 + K C^n} \tag{1}$$

where Q is the adsorbed amount with the rest being fitting constants from experimental data. A fitting model is usually required to interpolate the measured values. Also, the interpolation of the said data is quite sensitive to the choice of the fitting model and minute deviations from the true value can cause significant errors in thermodynamic calculations.[16,19]

### *Heats of adsorption*

At near ambient temperature, there is a negligible (3RT/2) difference between the sorbate–sorbent interaction energy and the experimental heats of adsorption.[2] For a basic understanding of the experimental results, the sorbate–sorbent interaction energies for the gas-sorbent pairs could be estimated by calculating the potential energies between the gas molecule and a free or isolated cation such as $Ca^{2+}$, $Li^+$, etc. A breakdown of the theoretical total sorbate–sorbent potential ($\phi_T$) for physical adsorption is shown in our previous work.[20] It is worth noting that for the adsorption of gas molecules on zeolites, the main interaction energies are between the gas molecules and the metal cations on its surface. Although interaction energies between the gas molecules and the oxide atoms on the surface also exists, they are significantly weaker than those formed with the cations.

Here-in, the isosteric heats of adsorption of the gas–sorbent pairings were estimated by the application of the Clausius–Clapeyron relation[17,18,21] as shown below:

$$\ln\left(\frac{P_1}{P_2}\right) = \frac{\Delta H_{vap}}{R}\left(\frac{1}{T_2} - \frac{1}{T_1}\right) \tag{2}$$

where $\Delta H_{vap}$ is the heat of adsorption, $R$ is the gas constant (8.3145 J/mol K), while $P_1$ and $P_2$ are the corresponding pressures at temperatures $T_1$ and $T_2$. Such calculations are very sensitive to errors in the equilibrium pressure. This means that interpolations can sometimes introduce significant uncertainties into the calculated isosteric heat determined by using fitted experimental data.

Figures 8 and 9 shows the isosteric heats of adsorption for $N_2$ and $O_2$ on various representative sorbents at different coverages. The $N_2$ experimental heats of adsorption followed the order: Ca-LSX > $Li_{2.5}Ca_{46.75}$-LSX > $Li_{4.2}Ca_{45.9}$-LSX > Li-LSX > Na-LSX.

The interaction energies for $N_2$ are mainly from the electrostatic energies. The interactions of $N_2$ with $Ca^{2+}$ are significantly stronger than that with $Li^+$. This is caused mainly by the higher electric charge of $Ca^{2+}$ that doubles the charge of $Li^+$, while the ionic radii are similar (0.69 Å for $Li^+$ and 1.0 Å for $Ca^{2+}$).

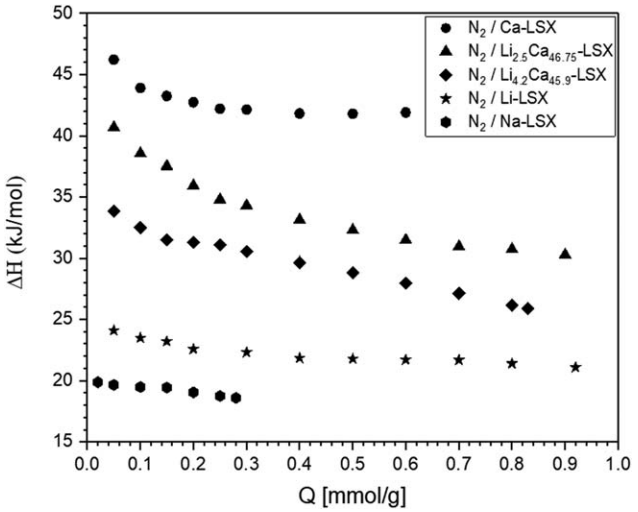


**Figure 8. $N_2$ heats of adsorption on various sorbents.**

An almost similar trend is observed for the $O_2$ experimental heats of adsorption Ca-LSX > $Li_{4.2}Ca_{45.9}$-LSX > $Li_{2.5}Ca_{46.75}$-LSX > Li-LSX > Na-LSX. As discussed in the foregoing, this trend was caused by the fact that $Ca^{2+}$ has a higher polarizability than $Li^+$ and the van der Waals interactions were the main interactions for adsorption of $O_2$.

### *Cation site location*

Table 1 shows the occupancy of cations in dehydrated X-type zeolites with pure cations. Several other studies have been employed to determine $Li^+$ in the extra framework of types X, Y, and A zeolites[5,6,22] using solid state NMR and neutron diffraction methods. The Li cations were found to be evenly distributed with 32 cations each in SI' (energetically preferred over SI for monovalent cations), SII, and SIII for the Li-LSX (Si/Al = 1) zeolite as opposed to 22 cations in SIII for the X-zeolite. Single Crystal XRD, Powder XRD, and Powder XRD & Neutron Diffraction have all been used to determine

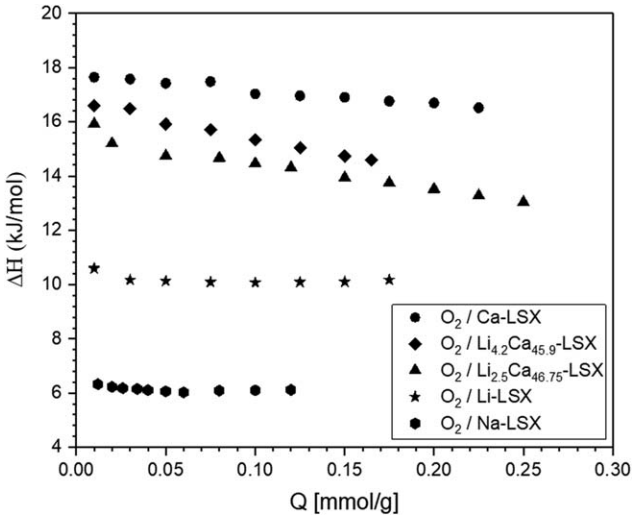


**Figure 9. $O_2$ heats of adsorption on various sorbents.**

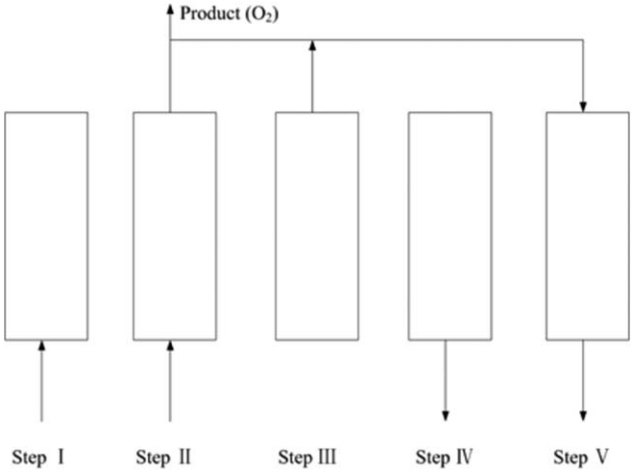


**Figure 10. PSA cycle configuration.**

the location of Ca ions mostly in Ca-X zeolites. It was found that for a fully dehydrated $Ca^{2+}$-exchanged FAU-type zeolite, the calcium cations were distributed among sites SI, SI′, and SII.[23–35]

No $Li^+$ and $Ca^{2+}$ location and site distribution studies were carried out in this study for the mixed-cation samples. Knowing that the SI and SI′ sites are sterically inaccessible to the sorbate gases ($N_2$ and $O_2$), it is therefore expected that only the Ca cations in SII and $Li^+$ in SIII are accessible to the sorbates.

For $N_2$ adsorption, as expected, the heats of adsorption followed the order: $Ca^{2+}$ (42 kJ/mol) > $Li^+$ (22 kJ/mol) > $Na^+$ (20 kJ/mol). It is most interesting that the $\Delta H$ values for the mixed LiCa-LSX samples fell between that of pure Ca-LSX and Li-LSX. This result was a strong indication that the $N_2$ molecules were interacting with both exposed Ca and exposed Li cations. Furthermore, the intermediacy of the $\Delta H$ value (between $Ca^{2+}$ and $Li^+$) indicates that some $N_2$ molecules were interacting with (or shared by) both $Ca^{2+}$ and $Li^+$ in possibly a bridged configuration.

Further work has been done in our laboratory on the relationship between SIII occupancy of $Li^+$ in mixed-cation LiNa-LSX zeolite and the heats of adsorption of $N_2$. It is shown that the $N_2$ heats of adsorption can indeed be used as an indicator of the presence of the lithium ions in SIII for mixed-cation zeolites (to be published).

### *PSA (or VPSA) cycle description*

A standard, commercially used, five-step PSA (or vacuum pressure swing adsorption, VPSA) cycle similar to that described by Hutson et al.[36] was used in this study. The cycle configuration is shown in Figure 10 and the five steps are as follows: (step I) pressurization with feed (air); (step II) high-pressure feed; (step III) co-current depressurization; (step IV) countercurrent blowdown; (step V) low-pressure purge with the product. This standard PSA cycle and even more complicated cycles can be accomplished in a two-bed or four-bed systems with interconnections.[37]

Each of the above steps ran for a duration of 30 s, thus the time required for the complete cycle was 2.5 min. The model assumed only two components (i.e., $O_2$ and $N_2$). Since Ar (Argon) and $O_2$ both have similar adsorption capacities on LSX zeolites, the oxygen component was assumed to be 22% (21% $O_2$ and 1% Ar) for the simulation. The product of each cycle was comprised of a volumetric mixture of the output stream from the feed step and the co-current depressurization step. A portion of this product stream was used to purge the other bed countercurrently in step V.

The performance of PSA for oxygen production is judged by three inter-related results: $O_2$ product purity, $O_2$ product recovery, and $O_2$ product throughput. When two of these are fixed, the other is also set provided the PSA operating conditions are optimized. To compare the performance of the sorbents developed in this work, the product throughputs of the sorbent were studied under several different cycle conditions.

Similarly, to facilitate a fair comparison of each sorbent's performance, the cycle conditions were optimized such that the product purity and product recovery obtained were the same for all sorbents in each simulation run. The product purity, product recovery, and product throughput in this study are defined as follows:

$$\text{Product Purity} = \frac{\text{Amount of } O_2 \text{ from Steps II and III}}{\text{Amount of } N_2 \text{ and } O_2 \text{ from Steps II and III}} \tag{3}$$

$$\text{Product Recovery} = \frac{(O_2 \text{ from Steps II and III}) - (O_2 \text{ from Step VI})}{(O_2 \text{ fed in Steps I and II})} \tag{4}$$

$$\text{Product Throughput} = \frac{\text{Amount of } O_2 \text{ produced per hour } \left({}^{t}/_{h}\right)}{\text{Amount of sorbent used in the bed (t)}} \tag{5}$$

The mathematical model and the numerical method used for the PSA simulations have been explained in detail in an earlier work by Rege and Yang[38] Hence, only the basic assumptions are listed here. The model used assumes the flow of a gaseous mixture of two components in a fixed bed packed with spherical adsorbent particles. The bed was considered to be adiabatic and the diffusional resistance is assumed to be negligible since the diffusion of $O_2$ and $N_2$ in the sorbents is relatively fast considering the long cycle time. Thus, local equilibrium existed between the gas and the solid phase for each gas component. Axial dispersion for mass and heat transfer was accounted for but dispersion in the radial direction is taken to be negligible. Axial pressure drop was neglected and ideal gas law was assumed to hold since pressures involved were near atmospheric. Also, the gas was assumed to have constant viscosity and heat capacity.

The pure component equilibrium amounts adsorbed on the respective adsorbents were fit using the well-known Langmuir-Freundlich isotherm with temperature-dependent constants. The equilibrium loading under mixture conditions were then predicted by the extended Langmuir-Freundlich equation in the simulation model:

$$q_k^* = \frac{q_{m_k} b_k p_k^{n_k}}{1 + \sum_{j=1}^{m} b_k p_k^{n_k}} \quad k = 1, 2 \tag{6}$$

The Langmuir-Freundlich parameters were assumed to be as follows:

$$q_m = k_1 e^{\left({}^{k_2}/_{T}\right)} \text{ and } b = k_3 e^{\left({}^{k_4}/_{T}\right)}$$

The extended Langmuir model is one of the simplest and most practical models for the prediction of binary gas adsorption behavior from pure component isotherms.[39] Using the

Table 3. Temperature-Dependent Parameters of Langmuir-Freundlich Isotherm of $N_2$ and $O_2$

| Sorbent | Sorbate | $k_1$ (mmol/g) | $k_2$ (K) | $k_3$ ($atm^{-1}$) | $k_4$ (K) | $N$ | $\Delta H$ (kJ/mol) |
|---|---|---|---|---|---|---|---|
| Li-LSX | $O_2$ | 0.4798 | 636.6 | 0.00948 | 500 | 1.08168 | 9.17 |
| Li-LSX | $N_2$ | 1.84559 | 139.68 | $2.19 \times 10^{-4}$ | 2484.2 | 1.033 | 21.79 |
| Ca-LSX | $O_2$ | 0.01448 | 1385.97 | 0.12788 | 207.35 | 1.152 | 12 |
| Ca-LSX | $N_2$ | 0.2623 | 646.75 | $6.88 \times 10^{-6}$ | 3785.11 | 0.931 | 43.39 |
| $Li_{2.5}Ca_{46.75}$-LSX | $O_2$ | 1.89933 | 145.55 | $6.20294 \times 10^{-4}$ | 1609.13 | 1.021 | 15.63 |
| $Li_{2.5}Ca_{46.75}$-LSX | $N_2$ | 1.31846 | 104.23 | $1.9726 \times 10^{-5}$ | 3489.63 | 0.958 | 31.47 |
| $Li_{4.2}Ca_{45.9}$-LSX | $O_2$ | 2.20255 | 179.35 | $4.02105 \times 10^{-4}$ | 1525.38 | 0.992 | 15.09 |
| $Li_{4.2}Ca_{45.9}$-LSX | $N_2$ | 0.98863 | 149.34 | $4.67445 \times 10^{-5}$ | 3243.35 | 0.999 | 28.72 |

extended Langmuir-Freundlich model for binary mixtures, similar to the use of the extended Langmuir model, is also a simple yet reasonably good way of fitting binary experimental data, as shown by Mulgundmath et al.[40]

The values of the Langmuir-Freundlich equation fitting constants and the heats of adsorption are shown in Table 3 while Table 4 shows the PSA bed characteristics and the operating conditions used.

### *VPSA simulation results*

The pressure ratio (ratio of the feed pressure $P_H$ to the desorption pressure $P_L$) is an important operating parameter for PSA systems. In this study, the feed pressure of 120 and 150 kPa with different pressure ratios were investigated and the same pressure ratios were employed for comparison of the studied sorbents.

A summary of the simulation conditions and separation results for the studied materials is given in Table S1 (in the Supporting Information). The feed and purge velocities were optimized so as to obtain the same product purity (near 95%) and recovery (near 52%) for all sorbents. Thus, the VPSA performance was judged by the $O_2$ productivities. Figures 11 and 12, which are both extracted from Table S1, shows the effect of pressure ratio on productivity for all four sorbents.

As can be seen from Figures 11 and 12, the higher the pressure ratio, the higher the productivity. It also shows that the $O_2$ productivity follows the following trend: (Li-LSX > $Li_{4.2}Ca_{45.9}$-LSX > $Li_{2.5}Ca_{46.75}$-LSX > Ca-LSX). The above result also justifies that Li-LSX is better than Ca-LSX for $O_2$ production and this is because the Ca-LSX zeolite has a higher heat of adsorption, higher $O_2$ capacity, and a lower $N_2$ working capacity. Upon comparison, the trend (Ca-LSX > $Li_{2.5}Ca_{46.75}$-LSX > $Li_{4.2}Ca_{45.9}$-LSX > Li-LSX) for the $N_2$ heats of adsorption for the four sorbents appears to be the reverse of the $O_2$ productivity above. Since adsorption is an exothermic process, the temperature in the bed will increase in the high-pressure feed step thereby affecting the $O_2$ separation results. It can be seen from the isotherms that the adsorption amount of $N_2$ on Ca-LSX is higher than that of the Li-LSX at 298 K. However, when the temperature is higher than 323 K, the adsorption amount of $N_2$ on Ca-LSX is lower compared to Li-LSX. Hence, the working capacity decreases sharply with increasing temperature for $N_2$ adsorption on Ca-LSX. A higher $N_2$ adsorption capacity could be achieved by employing a higher feed velocity at the same product purity and recovery. It is seen in Table S1 that Li-LSX has the highest feed velocity at the same simulation pressure.

The adsorption capacity of $O_2$ also has an important effect on PSA performance. When the $Li^+$ is exchanged into the Ca-

Table 4. Adsorption Bed Characteristics and Operating Conditions for PSA Simulations

| | |
|---|---|
| Bed length | 2.5 m |
| Diameter of sorbent | 1.0 m |
| Bed external porosity | 0.4 |
| Bed density | 720 $kg/m^3$ |
| Heat capacity of gases | 28.72 J/mol/K |
| Heat capacity of sorbent | 1.17 kJ/kg/K |
| Ambient temperature | 298 K |
| Feed gas temperature | 298 K |
| Feed gas composition | 78% $N_2$, 22% $O_2$ |
| Axial dispersion coefficient ($D_{ax}$) | $5 \times 10^{-5}$ $m^2/s$ |
| Effective heat conductive | 0.2 w/m/K |

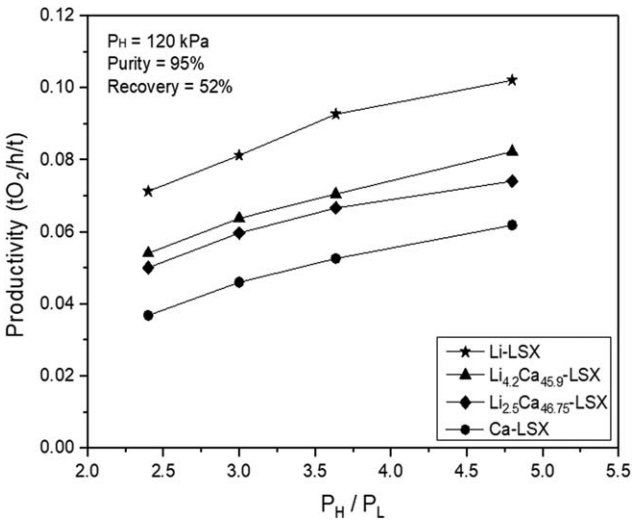


Figure 11. Comparison of $O_2$ productivity at 120 kPa pressure.

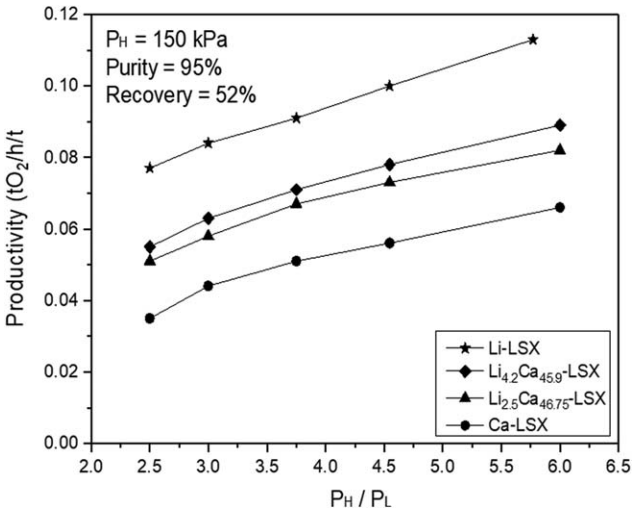


Figure 12. Comparison of $O_2$ productivity at 150 kPa pressure.

Table 5. Effects of $N_2$ Heats of Adsorption and $O_2$ Adsorption Capacity on PSA Performance

| Sorbent | $P_H$ (kPa) | $P_{CD}$ (kPa) | $P_L$ (kPa) | $U_H$ (m/s) | $U_L$ (m/s) | $O_2$ product purity (%) | $O_2$ product purity (%) | Product productivity ($tO_2$/h/t) |
|---|---|---|---|---|---|---|---|---|
| Ca-LSX@1 | 120 | 75 | 20 | 1.21 | 3.05 | 94.744 | 52.289 | 0.084 |
| (See text) | 120 | 80 | 25 | 1.13 | 2.27 | 94.995 | 51.903 | 0.0759 |
| | 120 | 80 | 33 | 0.99 | 1.59 | 95.238 | 52.146 | 0.0659 |
| | 120 | 85 | 40 | 0.92 | 1.21 | 95.307 | 51.992 | 0.0584 |
| | 120 | 90 | 50 | 0.802 | 0.85 | 94.971 | 51.821 | 0.0484 |
| Ca-LSX@2 | 120 | 75 | 20 | 1.04 | 2.8 | 94.959 | 52.426 | 0.0749 |
| (See Text) | 120 | 80 | 25 | 0.99 | 2.1 | 95.225 | 52.718 | 0.0684 |
| | 120 | 80 | 33 | 0.87 | 1.45 | 95.255 | 52.464 | 0.0578 |
| | 120 | 85 | 40 | 0.835 | 1.13 | 95.316 | 52.293 | 0.0519 |
| | 120 | 90 | 50 | 0.765 | 0.83 | 95.118 | 51.955 | 0.044 |

LSX zeolite, the oxygen adsorption capacity decreased in comparison with Ca-LSX. The decrease is beneficial because the lower the oxygen adsorption capacity, the better the PSA separation performance. In order to quantitatively study the effects of $N_2$ heats of adsorption and $O_2$ adsorption capacity on the separation results, the Ca-LSX zeolite was employed to simulate air separation by using, hypothetically, the $N_2$ heats of adsorption and $O_2$ isotherm of $Li_{4.2}Ca_{45.9}$-LSX, respectively. For simplicity purposes, Ca-LSX@1 and Ca-LSX@2 will be used to denote the sorbent pairings of Ca-LSX with $Li_{4.2}Ca_{45.9}$-LSX $N_2$ heats of adsorption and Ca-LSX with $Li_{4.2}Ca_{45.9}$-LSX $O_2$ isotherm, respectively.

All other simulation conditions were maintained except the high-pressure feed which was set at 120 kPa. The feed and purge velocities were also optimized so as to obtain the same product purity and recovery for both sorbents. Table 5 shows the simulation results while Figure 13 shows the separation results in comparison with the Ca-LSX and $Li_{4.2}Ca_{45.9}$-LSX sorbents. As can be seen from the result, the sorbent $Li_{4.2}Ca_{45.9}$-LSX has a higher $O_2$ productivity. Also, CaLSX@1 has a higher productivity than CaLSX@2. When the pressure ratio is 3, the $O_2$ productivity for sorbents CaLSX@1 and CaLSX@2 are 0.0584 $tO_2$/h/t and 0.0519 $tO_2$/h/t, respectively, which are 27 and 13% higher than that of pure Ca-LSX. The result also shows that the decrease in the $N_2$ heat of adsorption on $Li^+$-exchanged Ca-LSX has more contribution than the decrease in $O_2$ adsorption capacity to enhance $O_2$ productivity. As can be seen from Table 2, the $N_2$ heats of adsorption on Ca-LSX is 43.39 kJ/mol, which is much higher than that of $Li_{4.2}Ca_{45.9}$-LSX (28.72 kJ/mol). The detrimental effect of the heat of adsorption on the PSA performance is well illustrated by Lee et al.[41] in their development of heat-exchange PSA. Where significant improvement was shown in the PSA performance by using a two-bed PSA system in a shell-and-tube configuration that allowed heat transfer between the two beds. The effects of heats of adsorption/desorption are further complicated by their effects on the mass transfer rates[42] which can be significant in rapid or kinetically controlled PSA. In the PSA system under consideration, as mentioned above, mass transfer resistance was neglected due to the relatively long cycle time.

In commercial operation of VPSA, the operating high and low pressures are normally set as 150 and 50 kPa, respectively, for the production of $O_2$ via VPSA. With a pressure ratio of 3, it can be seen from Table S1 that when the feed pressure is 150 kPa, the $O_2$ productivity obtained using $Li_{4.2}Ca_{45.9}$-LSX is 0.0637 $tO_2$/h/t-sorbent compared to the throughput of 0.046 $tO_2$/h/t-sorbent and 0.084 $tO_2$/h/t-sorbent using Ca-LSX and Li-LSX, respectively. The corresponding $O_2$ product purity and recovery were approximately 95 and 52%. This shows that using the $Li_{4.2}Ca_{45.9}$-LSX sample enhanced $O_2$ productivity by 43% more than Ca-LSX, and only 25% lower than the productivity of Li-LSX. This is to say, in order to achieve the same $O_2$ productivity from using the $Li_{4.2}Ca_{45.9}$-LSX sorbent, one only has to increase the bed size by 1.32 times (or 32%). A similar trend was observed when the feed pressure was set at 120 kPa. The use of the mixed-cation LiCa-LSX results in savings of 70% lithium. Knowing that most of the fixed investments in VPSA $O_2$ production industry lies in the cost of the sorbent, these results present the possibility of considerable savings in capital and operating costs, especially with the steep rise in price (driven by the demand for rechargeable batteries) of lithium. Conversely, increasing the bed size factor would require larger vessels and larger compressors/vacuum blowers which should also be considered.

It should be noted that zeolitic sorbents used in industrial PSA/VSA processes are in the form of pellets that are formed with a clay binder, and the pelletized products need to be calcined in air at a high temperature. For example, in the improved sorbent (with high diffusion rates) of Ackley et al.,[43] the Li-LSX crystals were mixed with a clay binder to form pelletized beads and the beads needed to be calcined in dry air at up to 866 K for 3 h. Thus, for practical application of the

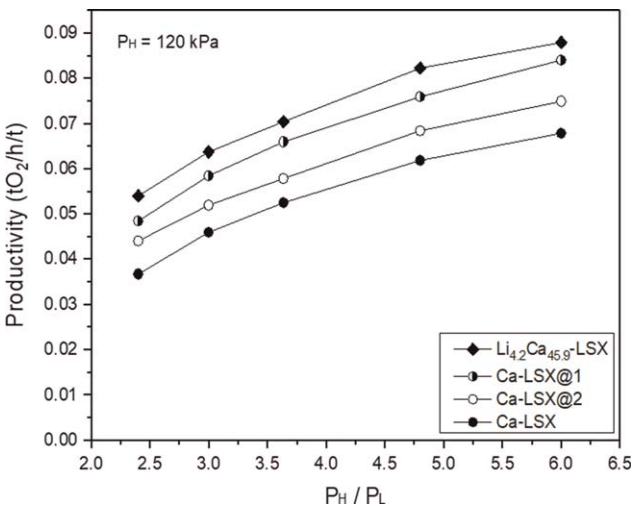


**Figure 13. Effect of $N_2$ heats of adsorption and $O_2$ isotherm on $O_2$ productivity.**

LiCa-LSX zeolite, a modification of the sample preparation steps is required. Pelletization of Ca-LSX with a binder followed by high temperature calcination will be performed first, which is to be followed by the Li ion exchange and mild calcination steps as described above. Ion exchange of zeolites in their pelletized form is practiced in laboratories[44] and, in fact, occurs in industrial wastewater treatment such as radioactive waste treatment.[45]

## Conclusion

Mixed-cation LiCa-LSX with less than 5% Li were prepared by sequential exchange (with Li exchange as the last step) followed by mild and short-time dehydration. Comparisons of adsorption isotherms of $N_2$ and $O_2$ and heats of adsorption data for the LiCa-LSX samples with that for pure-cation Li-LSX and Ca-LSX provided strong evidence that significant fractions of these $Li^+$ cations remained on the exposed exchange sites (SIII), thereby participating in adsorption of $N_2$ and $O_2$.

The mixed-cation LiCa-LSX samples were compared against the pure-cation Ca-LSX and Li-LSX based on their performance for oxygen production by PSA, via PSA model simulation. The simulation results show that the $Li_{4.2}Ca_{45.9}$-LSX sorbent with only a few Li cations exchanged into the pure Ca-LSX sample, could lead to significant improvements in the PSA production of $O_2$. This new exchange method shows a significant advantage over earlier research where more than 70% Li cations were exchanged with pure Na-LSX.[3,8,10,13]

## Literature Cited


1. Yang RT. *Gas Separation by Adsorption Processes*. London: Imperial College Press, 1997.
2. Yang RT. *Adsorbents: Fundamentals and Applications*. New Jersey: John Wiley & Sons, Inc., 2003.
3. Chao CC. Process for Separating Nitrogen from Mixtures Thereof with Less Polar Substances. US Patent 4,859,217, 1989.
4. Hutson ND, Yang RT. Structural effects on the adsorption of atmospheric gases in mixed Li,Ag–X-zeolite. *AIChE J*. 2000;46(11): 2305–2317.
5. Feuerstein M, Engelhardt G, McDaniel PL, MacDougall JE, Gaffney TR. Solid-state nuclear magnetic resonance investigation of cation siting in LiNaLSX zeolites. *Micropor Mesopor Mater*. 1998;26(1–3): 27–35.
6. Feuerstein M, Lobo RF. Characterization of Li cation in zeolite LiX by solid-state NMR spectroscopy and neutron diffraction. *Chem Mater*. 1998;10:2197–2204.
7. Olson DH, Sherry HS. An X-ray study of strontium-sodium ion exchange in Linde X. An example of a two-phase zeolite system. *J Phys Chem*. 1968;72:4095–4104.
8. Coe CG, Kirner JF, Pierantozzi R, White TR. Nitrogen adsorption with a Ca and/or Sr Exchanged Zeolite. US Patent 5,152,813, 1992.
9. Coe CG, Kirner JF, Pierantozzi R, White TR. Nitrogen adsorption with a divalent cation exchanged zeolite. US Patent 5,258,058, 1993.
10. Coe CG, Kirner JF, Pierantozzi R, White TR. Divalent cation exchanged Lithium X-zeolite for nitrogen adsorption. US Patent 5,417,957, 1995.
11. Coe CG, Kirner JF, Pierantozzi R, White TR. Zinc cation exchanged Lithium X-zeolite for nitrogen adsorption. US Patent 5,419,891, 1995.
12. Sircar S, Conrad RR, Ambs WJ. Binary ion exchanged type-X zeolite adsorbent. US Patent 4,557,736, 1985.
13. Chao CC, Sherman JD, Mullhaupt JT, Bolinger CM. Mixed ion-exchanged zeolites and processes for the use thereof in gas separations. US Patent 5,174,979, 1992.
14. Sircar S, Waldron WE. Oxygen production by adsorption. US Patent 0108494A1, 2002.
15. Hutson ND, Zajic SC, Yang RT. Influence of residual water on the adsorption of atmospheric gases in Li-X zeolite: experiment and simulation. *Ind Eng Chem Res*. 2000;39:1775–1780.
16. Mertens FO. Determination of absolute adsorption in highly ordered porous media. *Surf Sci*. 2009;603(10–12):1979–1984.
17. Mu B, Walton KS. Adsorption equilibrium of methane and carbon dioxide on porous metal-organic framework Zn-BTB. *Adsorption*. 2011;17(5):777–782.
18. Mu B, Schoenecker PM, Walton KS. Gas adsorption Study on Mesoporous Metal-Organic Framework UMCM-1. *J Phys Chem C*. 2010; 114:6464–6471.
19. Purewal J, Liu D, Sudik A, Veenstra M, Yang J, Maurer S, Müller U, Siegel DJ. Improved hydrogen storage and thermal conductivity in high-density MOF-5 composites. *J Phys Chem*. 2012;116(38): 20199–20212.
20. Epiepang FE, Li J, Liu Y, Yang RT. Low-pressure performance evaluation of $CO_2$, $H_2O$, and $CH_4$ on Li-LSX as a superior adsorbent for air prepurification. *Chem Eng Sci*. 2016;147:100–108.
21. Maly KE, Gagnon E, Wuest JD. Engineering molecular crystals with abnormally weak cohesion. *Chem Commun*. 2011;47(18):5163–5165.
22. Herden H, Einicke WD, Schollner R, Mortier WJ, Gellens LR, Uytterhoeven JB. Location of Li-ions in synthetic zeolites X and Y. *Zeolites*. 1982;2(2):131.
23. Bennett JM, Smith JV. Positions of cations and molecules in zeolites with the Faujasite-Type Framework I. Dehydrated Ca-exchanged faujasite. *Mat Res Bull*. 1968;3:633–642.
24. Sherry HS. The ion-exchange properties of zeolites. I. Univalent ion exchange in synthetic faujasite. *J Phys Chem*. 1968;70:1158–1168.
25. Vitale G, Bull LM, Morris RE, Cheetham AK, Toby BH, Coe CG, MacDougall JE. Combined neutron and X-ray Powder Diffraction Study of Zeolite Ca LSX and a $^2H$ NMR Study of Its Complex with Benzene. *J Phys Chem*. 1995;99:16087–16092.
26. Pluth JJ, Smith JV. Positions of cations and molecules in zeolites with the Faujasite-Type Framework VII. Dehydrated Ca-exchanged X. *Mat Res Bull*. 1972;7:1311–1322.
27. Pluth JJ, Smith JV. Positions of cations and molecules in zeolites with the Faujasite-Type Framework VIII. Dehydrated Ca-exchanged X. *Mat Res Bull*. 1973;8:459–468.
28. Costenoble ML, Mortier WJ, Uytterhoeven JB. Location of cations in synthetic zeolites-X and -Y Part 5: the cation distribution in Ca-Y, Ca-X and La-Y in the ultimate stages of dehydration. *J Chem Soc*. 1978;74:466–476.
29. Costenoble ML, Mortier WJ, Uytterhoeven JB. Location of cations in synthetic zeolites-X and -Y Part 6: the cation distribution in Ca-Y, Ca-X and La-Y in the ultimate stages of dehydration. *J Chem Soc*. 1978;74:477–483.
30. Smolin YI, Shepelev YF, Anderson AA. Atomic scale mechanism of CaX zeolite dehydration. *Acta Cryst*. 1989;45(2):124–128.
31. Jang SB, Jeong MS, Kim Y. Crystal structures of the ethylene and acetylene sorption complexes of fully $Ca^{2+}$-exchanged zeolite X. *J Phys Chem B*. 1997;101:3091–3096.
32. Yeom YH, Kim AN, Kim Y. Crystal structure of a benzene sorption complex of dehydrated fully $Ca^{2+}$-exchanged zeolite X. *J Phys Chem B*. 1998;102:6071–6077.
33. Jang SB, Jeong MS, Kim Y, Song SH, Seff K. Crystal structure of an ammonia sorption complex of dehydrated fully $Ca^{2+}$-exchanged zeolite X. *Micropor Mesopor Mater*. 1999;28:173–183.
34. Choi EY, Kim Y, Seff K. Crystal structure of a mesitylene sorption complex of dehydrated fully $Ca^{2+}$-exchanged zeolite X. Sorbed mesitylene appears to be significantly nonplanar. *J Phys Chem B*. 2002;106:5827–5832.
35. Jeong GH, Kim Y, Seff H. Crystal structure of a mesitylene sorption complex of dehydrated fully $Ca^{2+}$-exchanged zeolite X. $|Ca_{46}(CH_3NH_2)16|[Si_{100}Al_{92}O_{384}]$-FAU. *Langmuir*. 2004;20:9354–9359.
36. Hutson ND, Rege SU, Yang RT. Mixed cation zeolites: $Li_xAg_y$-X as a superior adsorbent for air separation. *AIChE J*. 1999;45(4):724–734.
37. Kim Y-H, Kim J-J, Lee C-H. Adsorptive cyclic purification process for $CO_2$ mixtures captured from coal power plants. *AIChE J*. 2017; 63:1051–1063.
38. Rege SU, Yang RT. Limits for air separation by adsorption with LiX zeolite. *Ind Eng Chem Res*. 1997;36:5358–5365.
39. Kennedy DA, Mujcin M, Trudeau E, Tezel FH. Pure and binary adsorption equilibria of methane and nitrogen on activated carbons, desiccants, and zeolites at different pressures. *J Chem Eng Data*. 2016;61(9):3163–3176.
40. Mulgundmath VP, Tezel FH, Hou F, Golden TC. Binary adsorption behavior of methane and nitrogen gases. *J Porous Mater*. 2012;19(4):455–464.

41. Lee J-J, Kim M-K, Lee D-G, Ahn H-W, Kim M-J, Lee C-H. Heat-exchange pressure swing adsorption process for hydrogen separation. *AIChE J*. 2008;54(8):2054–2064.
42. Wang Y, LeVan MD. Master curves for mass transfer in bidisperse adsorbents for pressure-swing and volume-swing frequency response methods. *AIChE J*. 2011;57(8):2054–2069.
43. Ackley MW, Barrett PA, Stephenson NA, Kikkinides ES. High rate compositions. US Patent 0340612A1, 2013.
44. Moura PAS, Bezerra DP, Vilarrasa-Garcia E, Bastos-Neto M, Azevedo DCS. Adsorption equilibria of $CO_2$ and $CH_4$ in cation-exchanged zeolites 13X. *Adsorption*. 2016;22(1):71–80.
45. Breck DW. *Zeolite Molecular Sieves: Structure, Chemistry, and Use*. Malabar, FL: RE Krieger, 1984:529–588.

*Manuscript received Aug. 2, 2017, and revision received Oct. 6, 2017.*